LANGMUIR

Article

pubs.acs.org/Langmuir

A Self-Assembled Ratiometric Polymeric Nanoprobe for Highly Selective Fluorescence Detection of Hydrogen Peroxide

Chongchong Feng,[†] Fengyang Wang,[†] Yijing Dang,[†] Zhiai Xu,*[,†] Haijun Yu,[‡] and Wen Zhang[†]

[†]School of Chemistry and Molecular Engineering, East China Normal University, Shanghai 200241, People's Republic of China

[‡]Center of Pharmaceutics, Shanghai Institute of Materia Medica, Chinese Academy of Sciences, Shanghai 201203, People's Republic of China

Supporting Information

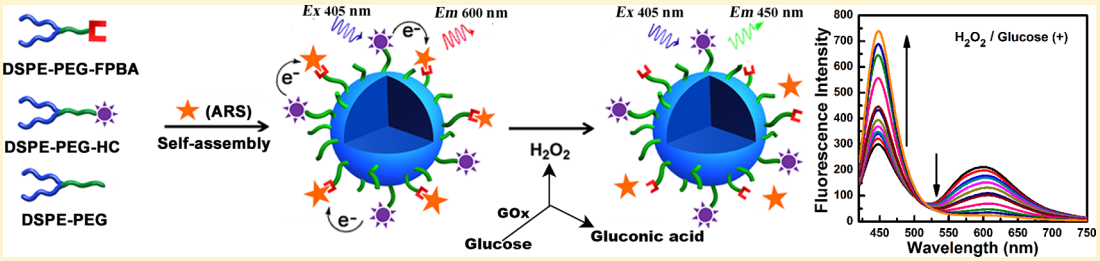

ABSTRACT: In this study, a dual-emission fluorescence resonance energy transfer (FRET) polymeric nanoprobe by single-wavelength excitation was developed for sensitive and selective hydrogen peroxide (H_2O_2) detection. Polymeric nanoprobe was prepared by simple self-assembly of functional lipopolymers, which were 4-carboxy-3-fluorophenylboronic acid (FPBA)-modified DSPE-PEG (DSPE-PEG-FPBA) and 7-hydroxycoumarin (HC)-conjugated DSPE-PEG (DSPE-PEG-HC). Subsequent binding of alizarin red S (ARS) to FPBA endowed the nanoprobe with a new fluorescence emission peak at around 600 nm. Because of the perfect match of the fluorescence emission spectra of HC with the absorbance spectra of ARS-FPBA, FRET was achieved between them. The sensing strategy for H_2O_2 was based on H_2O_2-induced deboronation reaction and boronic acid-mediated ARS fluorescence. Interaction between phenylboronic acid and ARS was revisited herein and it was found that electron-donating or -withdrawing group on phenylboronic acid (PBA) has significant influence on the fluorescence property of ARS, which enabled sensitive and selective H_2O_2 sensing. The nanoprobe displayed two well-separated emission bands (150 nm), providing high specificity and sensitivity for ratiometric detection of H_2O_2. Further application was exploited for the determination of glucose and the results demonstrated that the proposed strategy showed ratiometric response capability for glucose detection. The current method does not involve complicated organic synthesis and opens a new avenue for the construction of multifunctional polymeric fluorescent nanoprobe.

INTRODUCTION

Hydrogen peroxide (H_2O_2) is a crucial biochemical molecule, which plays a significant role in cellular signal transduction.[1−4] In the presence of O_2 and enzymes, lots of biological substrates can be specifically catalyzed to produce H_2O_2 as a byproduct.[5] However, excessive presence of H_2O_2 is associated with oxidative stress and serious cell damage, leading to pathogenic states such as inflammation, cancer, cardiovascular diseases, and neurodegenerative disorders.[6,7] Therefore, extensive efforts have been devoted for selective and sensitive detection of H_2O_2.[8−11] Among the various modalities, fluorescence detection is a fascinating method characterized by fast response, high sensitivity, and compatible with microscopic technique.[12−16] Although some fluorescent probes have been developed in recent years, the majority of them offer single-emission fluorescent signal, which may lead to inaccurate quantification. Ratiometric fluorescent probes that can exhibit strong anti-interference ability and afford high contrast images are favorable for H_2O_2 detection in biological environment.[17−19] In particular, ratiometric probes with large emission shift upon single-wavelength excitation are highly desired.

In past years, nanomaterial-based ratiometric fluorescent probes have drawn increasing interests owing to their remarkable advantages including their nanosize, good photostability, and rich functional groups for further modification.[20−22] The polymeric micelle is one promising nanosystem receiving much attention in many fields especially that of drug delivery as carriers of diagnostic and therapeutic agents.[23−25] Polymeric micelles are usually core−shell structures formed by self-assembly of amphiphilic block copolymers present with attractive features, such as good solubility and prolonged blood circulation.[26−30] In addition, they offer the benefit of high versatility in terms of composition and functionality, providing high potential for designing nanoprobes for bimolecular detection.

Received: January 18, 2017
Revised: March 20, 2017

DOI: 10.1021/acs.langmuir.7b00189
Langmuir XXXX, XXX, XXX−XXX

Scheme 1. Schematic Illustration of the Self-Assembled FRET Polymeric Nanoprobe Based on ARS-FPBA for Ratiometric Detection of H_2O_2

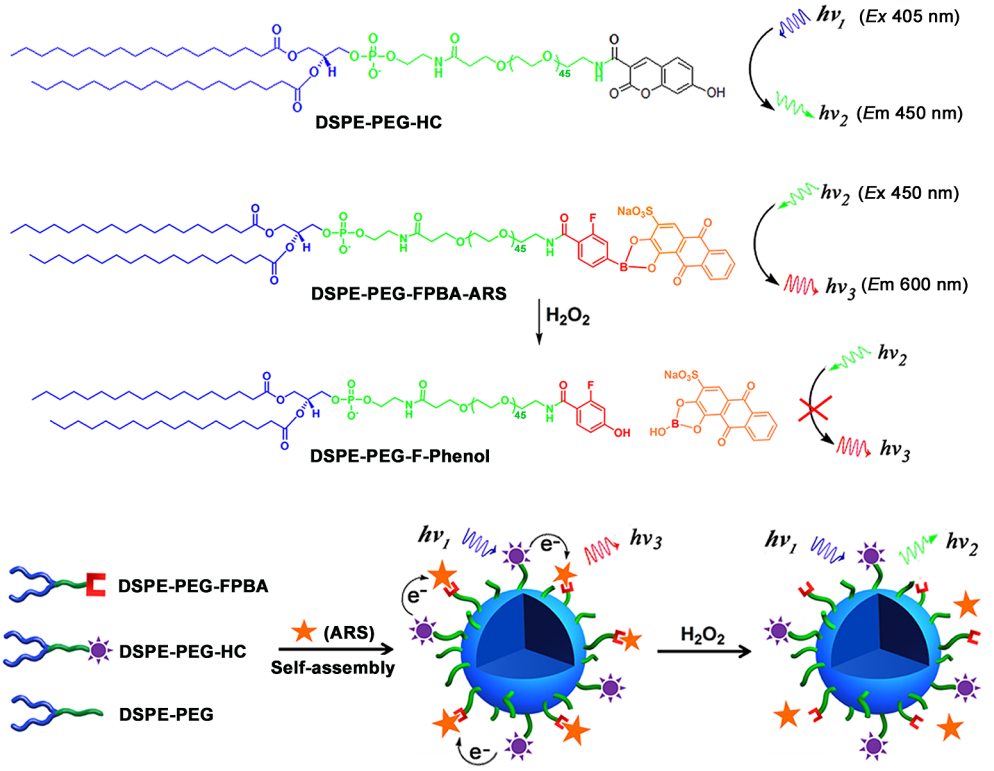

Alizarin red S (ARS) is a readily available dye which is nearly nonfluorescent due to the excited state proton transfer quenching.[31,32] Its fluorescence intensity increases dramatically upon forming adducts with boronic acid derivatives.[33] This excellent property was adopted for many fluorescent sensing applications including mainly carbohydrates based on their competitive binding to boronic acid derivatives.[34−36] However, the applications are limited and they usually give turn-off fluorescence responses. In this study, by screening boronic acid derivatives with the absorbance and fluorescence spectra we found that the fluorescence response to H_2O_2 was dependent on the functional group on phenylboronic acid (PBA) and the response was sensitive and highly selective in the case of 4-carboxy-3-fluorophenylboronic acid (FPBA). To the best of our knowledge, there is little to no information in the literature about utilizing ARS-boronate composite for H_2O_2 sensing. Moreover, it does not involve complicated synthesis and purification processes. On the basis of the self-assembly method, we developed a fluorescence resonance energy transfer (FRET) polymeric nanoprobe with dual-emission for highly selective detection of H_2O_2 by modifying FPBA and 7-hydroxycoumarin-3-carboxylic acid (HC) on lipopolymer 1,2-distearoyl-*sn*-glycero-3-phosphoethanolamine-*N*-[amino-(polyethylene glycol)-2000] (DSPE-PEG-NH_2). The nanoprobe was successfully used to determine H_2O_2 ratiometrically with two well-separated emissions upon single-wavelength excitation, and the fluorescence detection of glucose based on enzyme-catalyzed H_2O_2 production was realized. This developed method was facile, highly selective, and promising as a candidate for detection of H_2O_2 and H_2O_2-related substances.

EXPERIMENTAL SECTION

Chemicals and Reagents. FPBA, ARS, 2,2-azobis(2-methylpropionamidine) dihydrochloride (AAPH), potassium dioxide (KO_2), and boric acid (BA) were all purchased from Aladdin reagent company (Shanghai, China). Glucose oxidase (GOx), 4-carboxyphenylboronic acid (4-CPBA, 98%), 4-mercaptophenylboronic acid (TPBA, 90%), 3-(2-hydroxy-1-methylethyl-2-nitrosohydrazino)-1-propanamine (NOC5), fructose, galactose, sucrose, maltose, anhydrous glucose, *N*-acetylneuraminic acid (SA), and fetal bovine serum (FBS) were all purchased from Sigma-Aldrich (Shanghai, China). PBA (99%), 3-aminophenylboronic acid (APBA, 98%), 3-carboxyphenylboronic acid (3-CPBA, 98%), 1-hydroxybenzotriazole anhydrous (HOBT, 98%), and *N*-(3-(dimethylamino)propyl)-*N*′-ethylcarbodiimide hydrochloride (EDCI, 99%) were all purchased from J&K Scientific Ltd. (Shanghai, China). 7-Hydroxycoumarin-3-carboxylic acid (HC, >98%) was purchased from TCI Co., Ltd. (Shanghai, China). 1,2-Distearoyl-*sn*-glycero-3-phosphoethanolamine-*N*-[amino(polyethylene glycol)-2000] (DSPE-PEG-NH_2) was purchased from Shanghai A. V. T. Pharmaceutical L.T.D. Co. (Shanghai, China). HEPES buffer (25 mM, pH 7.4) and Milli-Q water were used throughout the whole study. Dialysis tubes with a molecular weight cutoff of 1000 Da (MWCO 1000 Da) were obtained from Spectrum Laboratories, Inc. (CA, U.S.A.).

Measurements. The UV−vis absorption and fluorescence spectra were measured with a Cary 60 UV−vis spectrophotometer and a Cary Eclipse spectrofluorophotometer, respectively (Agilent Technologies, CA, U.S.A.). ^{1}H NMR of DSPE-PEG-HC and DSPE-PEG-FPBA were measured by using a Bruker-400 MHz NMR spectrometer at 25 °C. The dynamic light scattering (DLS) measurement was measured at 25 °C using a Malvern zetasizer Nano ZS (ZS90, Malvern, U.K.). Transmission electron microscope (TEM) image was obtained with a JEOL JEM-2100 microscopy (JEOL, Tokyo, Japan). The mass spectrometry was conducted by a Micromass Q-TOF Ultima mass spectrometer (Waters, Manchester, U.K.). Fluorescence lifetime measurements were performed on a FLS980 fluorescence spectrometer from Edinburgh Instruments Ltd. (Photonics Division, U.K.).

DOI: 10.1021/acs.langmuir.7b00189
Langmuir XXXX, XXX, XXX−XXX

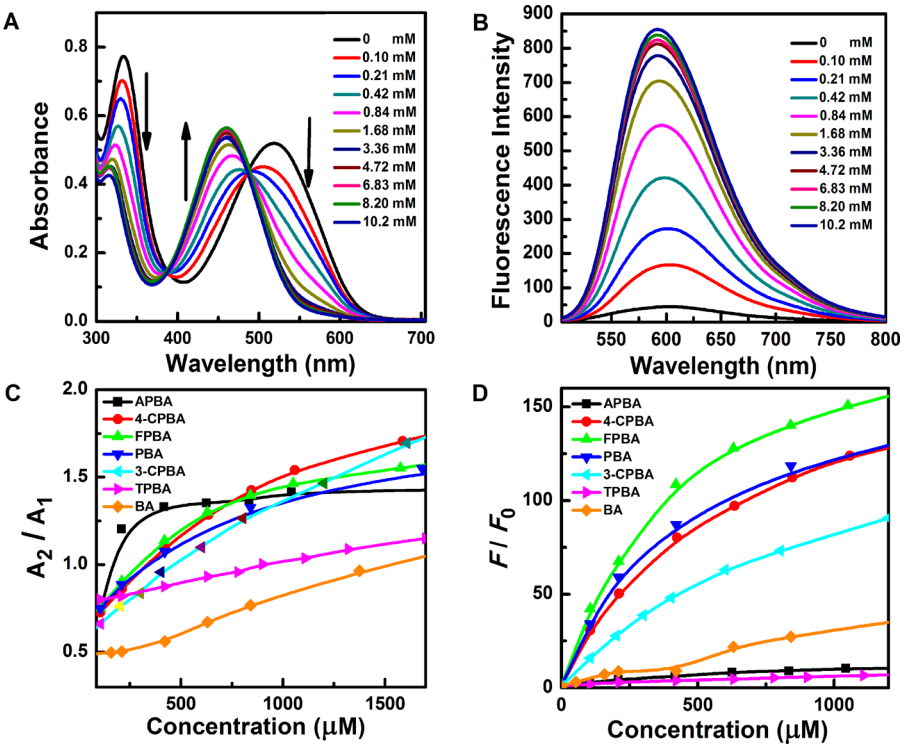

Figure 1. Absorbance (A) and fluorescence (B) spectra of ARS in the presence of different concentrations of PBA (λ_{ex} = 488 nm). (C) Ratiometric change of ARS absorbance (A_2/A_1) in the presence of BA or PBA derivatives. (D) Fluorescence intensity change at 600 nm as a function of BA or PBA derivatives concentration in the range of 0−1.2 mM. (F_0, the fluorescence intensity of ARS; F, the fluorescence intensity of ARS-BA and ARS-PBA derivatives; [ARS] = 0.1052 mM.).

Synthesis of DSPE-PEG-FPBA and DSPE-PEG-HC. First, FPBA was dissolved in DMSO and activated by EDCI and HOBT for 2 h (FPBA/EDCI/HOBT = 1:1.2:1.2, mol/mol/mol). Second, DSPE-PEG-NH_2 was dissolved in DMSO, mixed with TEA (DSPE-PEG-NH_2/TEA/FPBA = 1:3:3, mol/mol/mol) and stirred for 2 h. Then, FPBA solution was dropwise added to the solution of DSPE-PEG-NH_2, reacted at room temperature for 24 h. The mixture was dialyzed for 72 h to remove unreacted impurities and then lyophilized. The chemical structure of DSPE-PEG-FPBA was confirmed by ^{1}H NMR spectra. ^{1}H NMR (500 MHz, DMSO-d_6, δ): 7.63 (s, 1H), 7.57 (s, 1H), 6.53 (s, 1H), 5.64 (s, 1H), 5.10−5.06 (m, 1H), 4.28 (s, 1H), 3.86 (s, 6H),3.80−3.67 (m, 5H), 3.65 (s, 8H), 3.62−3.48 (m, 72H), 3.44−3.34 (m,6H), 3.32 (s, 20H), 3.09−3.05 (m, 1H), 2.64 (s, 12H), 2.54−2.47 (m,73H), 2.37 (s, 2H), 2.28−1.45 (m, 25H), 1.50 (s, 13H), 1.50 (s, 18H), 1.24 (s, 22H), 1.15 (s, 1H), 0.86 (t, J = 6.7 Hz, 23H), 0.01 (s, 3H).

DSPE-PEG-HC was synthesized by following a similar procedure as that of DSPE-PEG-FPBA. The chemical structure of DSPE-PEG-HC was confirmed by ^{1}H NMR spectra. ^{1}H NMR (500 MHz, DMSO-d_6, δ): 9.17 (s, 1H), 8.79−8.75 (m, 1H), 8.30 (s, 1H), 8.21 (s,1H), 8.17−8.13 (m, 1H), 8.08−8.04 (m, 1H), 7.91 (s, 1H), 7.48 (d, J = 8.3 Hz, 1H), 7.38 (dd, J = 21.5, 14.0 Hz, 2H), 7.22 (s, 1H), 7.16 (d, J = 9.0 Hz, 1H), 6.97 (s, 1H), 6.92 (s, 1H), 6.06 (s, 1H), 5.74 (s, 1H), 4.30 (s, 20H), 4.28 (s, 24H), 4.18 (d, J = 99.1 Hz, 29H), 3.75 (d, J = 93.8 Hz, 5H), 3.86−3.48 (m, 29H), 3.42 (s, 1H), 3.31 (d, J = 11.6 Hz, 13H), 3.22 (s, 1H), 2.89 (s, 1H), 2.64 (s, 3H), 2.51 (s, 62H), 2.37 (s, 1H), 2.26 (s, 1H), 2.11−2.07 (m, 1H), 1.51−1.47 (m, 1H), 1.24 (s, 8H), 1.15 (s, 3H), 0.86 (t, J = 6.8 Hz, 2H), 0.01 (s, 3H).

Preparation of the Ratiometric Nanoprobe. The ratiometric nanoprobe was prepared through a film hydration process. Briefly, 9 mg of DSPE-PEG, 1 mg of DSPE-PEG-FPBA, and 0.005 mg of DSPE-PEG-HC were mixed in 5 mL of chloroform. Then the solution was evaporated to remove chloroform. Five milliliters of HEPES buffer (25 mM, pH 7.4) was added to the round-bottom flask and sonicated for 30 min. One milliliter of micelle solution was mixed with 1 mL of ARS solution (0.6 mM). The impurities were then separated from the solution by dialysis (MWCO: 1000 Da) for 2 h.

The Stability of the Ratiometric Nanoprobe. The stability of the nanoprobe was assessed by monitoring the change of micellar size under simulative physiological conditions. In brief, the micellar solution was mixed with an equal volume of HEPES buffer (25 mM, pH 7.4) and medium containing 10% fetal bovine serum (FBS). The mixtures were incubated at 37 °C for different times and determined by DLS.

Glucose Detection. Glucose detection was performed as follows: 6 μL of 2 mg/mL GOx, 6 μL of different concentrations of glucose and 18 μL of HEPES buffer (25 mM, pH 7.4) were incubated at 37 °C for 30 min. Then 30 μL of the nanoprobe solution was injected into the resulting solution and allowed to incubate further for 1 h. Subsequently, the fluorescence signal of the mixtures was recorded.

The detection of glucose in fetal bovine serum was carried out as follows: the fetal bovine serum was first treated with 10 mg/mL GOx for 12 h at 37 °C. Then, glucose with varying concentrations was spiked into the pretreated fetal bovine serum. Then, the glucose detection was carried out according to the procedure as mentioned above.

RESULTS AND DISCUSSION

Polymeric micelles are unique nanostructures that can integrate multifunctionalities such as recognition, detection, and drug delivery. DSPE-PEG is a biocompatible amphiphilic polymer. Herein, we utilize DSPE-PEG to construct a ratiometric fluorescent nanoprobe for H_2O_2 detection by conjugating FPBA and HC on DSPE-PEG polymer (Scheme 1). The detection strategy is based on H_2O_2-induced deboronation reaction and boronic acid-mediated ARS fluorescence. As illustrated in Scheme 1, DSPE-PEG-FPBA, DSPE-PEG-HC, and DSPE-PEG can self-assemble to form the polymeric nanoprobe. In the absence of ARS, the polymeric nanoprobe

DOI: 10.1021/acs.langmuir.7b00189
Langmuir XXXX, XXX, XXX−XXX

displays a blue-colored fluorescence with an emission peak at 450 nm from HC upon excitation at 405 nm. After ARS is added into the micelle solution, it interacts with FPBA and FRET could occur between ARS-FPBA and HC with the appearance of a new fluorescence emission peak at 600 nm. However, in the presence of H_2O_2, ARS would dissociate from the nanoprobe surface and result in the decrease of fluorescence intensity at 600 nm and increase of fluorescence intensity at 450 nm, allowing a ratiometric fluorescence response for the detection of H_2O_2 by single-wavelength excitation.

It is known that ARS can form adducts with boronic/boric acid and ARS shows great fluorescence enhancement upon binding.[37] Herein, we revisit this reaction by examining the absorption and fluorescence spectra of ARS in the presence of different boronic acid derivatives. As an example, Figure 1A shows the absorption spectra of ARS in the absence and presence of various concentrations of PBA. ARS displays two obvious absorbance bands with peaks located at 333 and 510 nm in the range of 300−700 nm. Upon the addition of PBA, the absorption at 333 nm declines significantly with a slight blue-shift. The absorption peak at 510 nm blue shifts to 460 nm gradually and the absorbance intensity decreases first but increases later. Two isosbestic points at 386 and 488 nm appear, indicating ARS and PBA have formed a stable compound. Figure 1B shows the corresponding fluorescence spectra of ARS without or with different concentrations of PBA. This result clearly reflects that ARS has very weak fluorescence emission but upon interaction with PBA, its fluorescence increases rapidly with the maximum emission wavelength blue shifting from 600 to 590 nm. To better understand the interaction of ARS with boronic acid derivatives, we studied six PBA derivatives together with BA by measuring the absorbance and fluorescence spectra. As shown in Figure 1C, A_1 is the declined intensity of absorbance peak at about 510 nm and A_2 is the increased intensity of absorbance peak at about 460 nm. By increasing the concentration of BA or PBA derivatives, A_2/A_1 rises rapidly and tends to approach constant at higher concentration. In particular, the A_2/A_1 ratio of ARS-APBA approaches constant quickly while ARS-TPBA keeps gradual increase all through the investigated concentration range. Accordingly, a significant color change from pink to orange was observed in the presence of PBA derivatives (Figure S1, Supporting Information). The change in fluorescence is plotted against BA or PBA derivatives concentration (Figure 1D). Upon the addition of different concentrations of BA or PBA derivatives to the solution of ARS, BA and six PBA derivatives behave similarly, whereas the fluorescence enhancement differs greatly. For instance, there is about 150-fold fluorescence increase (F/F_0) for FPBA but only a 10-fold increase is observed for that of APBA. We propose that the disparity of the enhancement on ARS fluorescence originates from the difference of the substitution groups on phenyl ring. Carboxyl and fluorine are electron-withdrawing groups that are better at preventing the excited state proton transfer quenching of ARS than electron-donating groups, such as amino and thiol groups. Additionally, the difference of F/F_0 between ARS-3-CPBA and ARS-4-CPBA indicates that para-substituent is better for fluorescence enhancement.

The binding affinity of ARS with BA and PBA derivatives was analyzed by nonlinear least-squares regression with the following equations[38,39]

$$\frac{F}{F_0} = \frac{\{1 + kK[\mathrm{B}]\}}{\{1 + K[\mathrm{B}]\}} \quad (1)$$

where F and F_0 are the fluorescence intensities of ARS in the presence and absence of BA or PBA derivatives, respectively, and k ($= k_c/k_L$) represents the ratio of proportionality constants connecting the fluorescence intensity and concentrations of the species (complex, k_c; free ligand, k_L). K is the binding constant for complexation of ARS with BA or PBA derivatives. The free BA or PBA derivatives concentration, [B], can be related to known total concentrations of BA or PBA derivatives concentration (B_0) and ligand (L_0), by the following equation

$$B_0 = [\mathrm{B}] + \frac{\{L_0K[\mathrm{B}]\}}{\{1 + K[\mathrm{B}]\}} \quad (2)$$

Together, eqs 1 and 2 describe the system. The data in Figure 1D can be fitted well with the equations and Table 1 shows the results of the binding constant of ARS with BA or PBA derivatives. The sequence of binding constant is FPBA > PBA > 4-CPBA > APBA > 3-CPBA> TPBA > BA.

Table 1. Binding Constant of ARS with BA or PBA Derivatives

	PBA	APBA	4-CPBA	3-CPBA	TPBA	FPBA	BA
binding constant (M^{-1})	2624	1713	1860	1121	715	2804	213

According to previous studies, boronic groups in boronate-derivatized organic compounds can be transformed into phenol upon the reaction with H_2O_2.[40,41] We deduce that ARS-PBA derivatives can be used to detect H_2O_2. The spectroscopic properties of ARS-PBA derivatives after reaction with H_2O_2 were investigated in HEPES buffer (25 mM, pH 7.4). As shown in Figure 2A,B, UV−vis spectra indicates that the absorption peak of ARS-FPBA at 510 nm red shifts to 515 nm with slight enhancement along with the increase of H_2O_2 concentration. The fluorescence spectra shows that the fluorescence intensity of ARS-FPBA decreases with the H_2O_2 concentration increase ranging from 0 to 500 μM. The fluorescence change of ARS-FPBA (F/F_0) at 600 nm is plotted in Figure 2C and it shows that F/F_0 quickly decreases and levels off when the concentration of H_2O_2 is above 500 μM. The reaction of ARS-FPBA with H_2O_2 transformed boronates into phenols with concomitant dissociation of BA and ARS (Scheme S1, Supporting Information). FPBA shows much higher enhancement on ARS fluorescence than BA, therefore, H_2O_2-induced deboronation reaction leads to decreased fluorescence response. To support the above-mentioned mechanism, the solution of ARS-FPBA before and after reaction with H_2O_2 were detected by mass spectrometry (MS). Upon reaction with H_2O_2, a new peak ascribed to 4-carboxy-3-fluorophenol appeared (Figure S2, Supporting Information).

As expected, the fluorescence intensity of ARS-CPBA and ARS-FPBA both decreases upon reaction with H_2O_2. In obvious contrast, the fluorescence intensity of ARS-BA is almost unchanged in the presence of H_2O_2 but that of ARS-APBA is enhanced. Similarly, after reacting with H_2O_2, F/F_0 of ARS-TPBA has a trend of rise, while the subsequent decline may be explained by the susceptibility of thiol group to be oxidized (Figure 2D). Therefore, the variation in fluorescence

DOI: 10.1021/acs.langmuir.7b00189
Langmuir XXXX, XXX, XXX−XXX

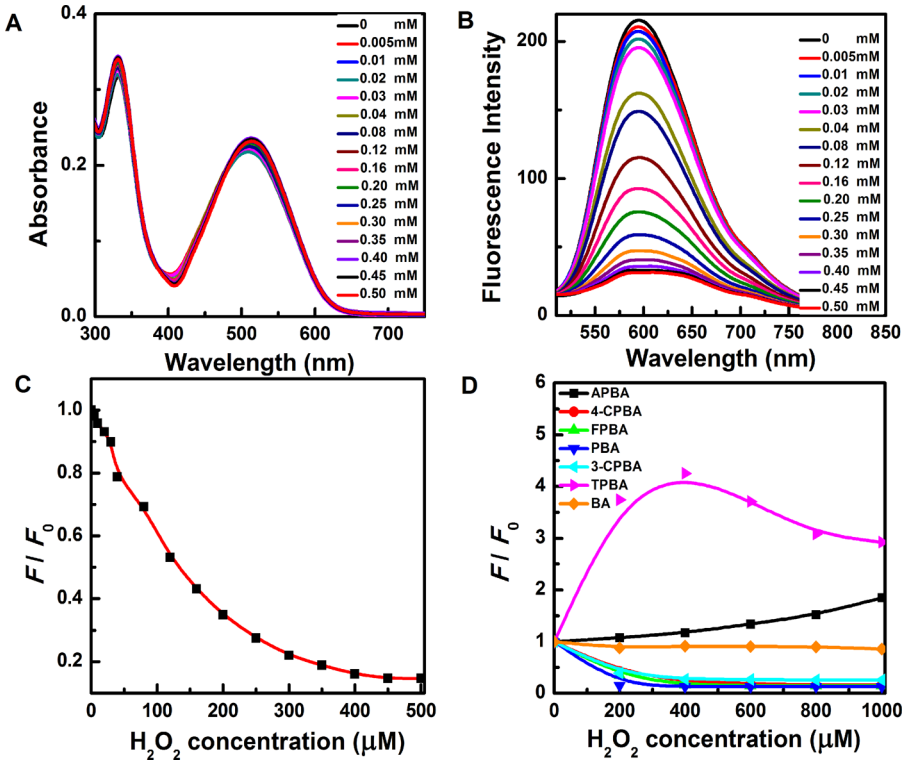

Figure 2. (A) Absorbance and (B) fluorescence spectra of ARS-FPBA in the presence of different concentrations of H_2O_2. (C) Fluorescence intensity change of ARS-FPBA at 600 nm as a function of H_2O_2 concentration. ([ARS] = 0.0526 mM, [FPBA] = 0.0526 mM). (D) The fluorescence intensity change of ARS-BA or ARS-PBA derivatives with the addition of different concentrations of H_2O_2. (F_0, the fluorescence intensity without addition of H_2O_2; F, the fluorescence intensity with addition of H_2O_2).

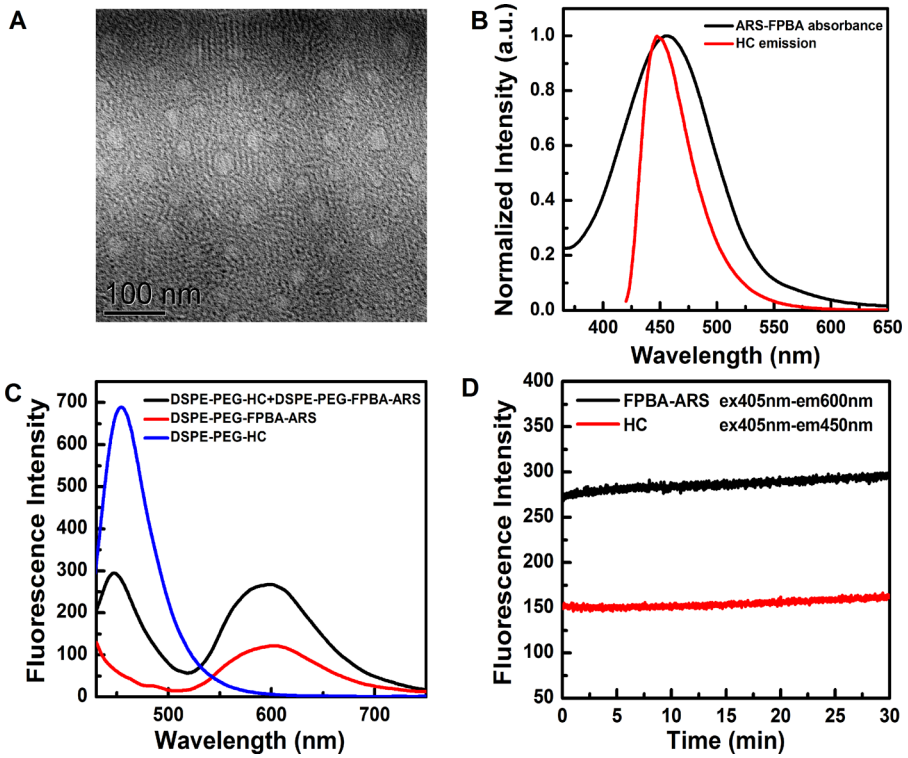

Figure 3. (A) The TEM image of the micelle nanoparticles. The scale bar corresponds to 100 nm. (B) Absorption spectra of ARS-FPBA and emission spectra of HC. (C) The fluorescence spectra of different polymeric nanoprobes. (λ_{ex} = 405 nm). (D) Fluorescence photostability of the polymeric nanoprobe in HEPES buffer solution (25 mM, pH 7.4).

DOI: 10.1021/acs.langmuir.7b00189
Langmuir XXXX, XXX, XXX−XXX

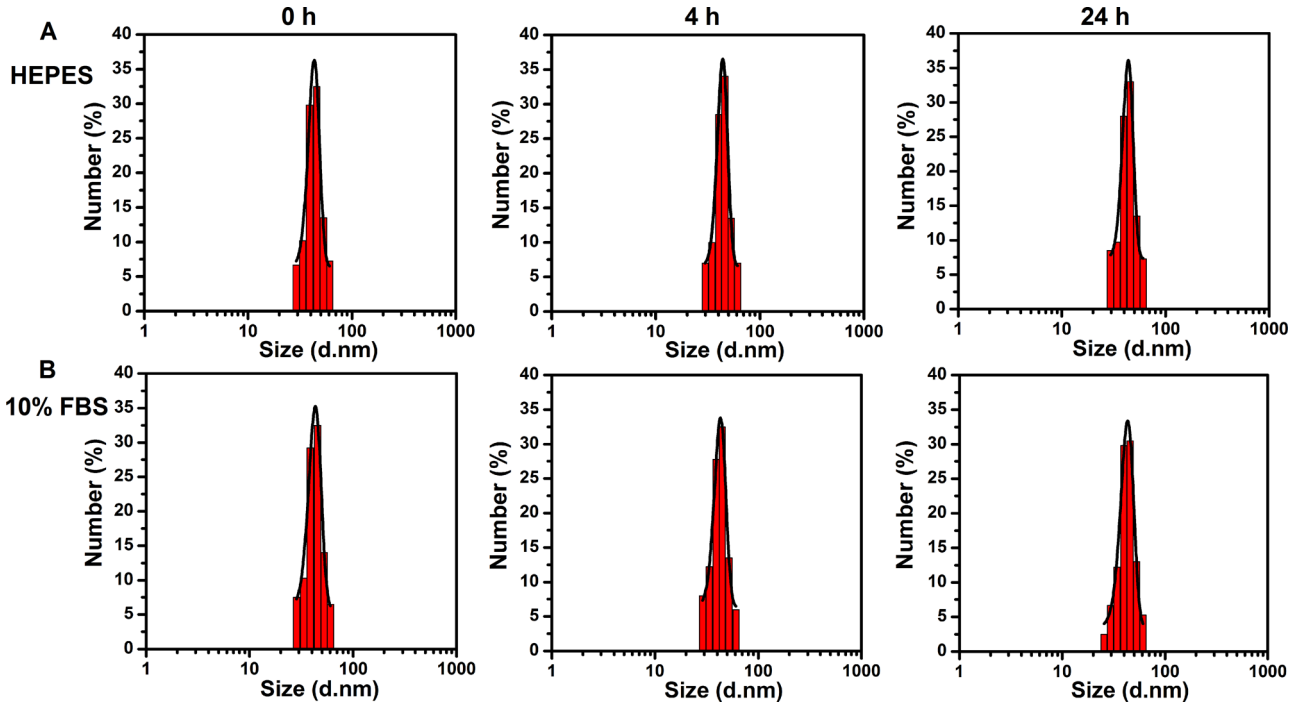

Figure 4. Stability of the polymeric nanoprobe in (A) HEPES buffer solution (25 mM, pH 7.4) and (B) HEPES buffer solution (25 mM, pH 7.4) containing 10% FBS studied by dynamic light scattering experiment.

intensity for different PBA derivatives allows us to rationally design H_2O_2-responsive fluorescent probe, and FPBA was chosen for the construction of the nanoprobe.

HC and FPBA was conjugated with DSPE-PEG-NH_2 through condensation reaction between amino and carboxyl group (Scheme 1 and S2, Supporting Information). The successful synthesis of them was verified by ^{1}H NMR spectra (Figure S3, Supporting Information). Next, we prepared the polymeric nanoprobe by hybrid self-assembly of DSPE-PEG, DSPE-PEG-HC and DSPE-PEG-FPBA through a film hydration process. Transmission electron microscope (TEM) image shows that the micelle nanoparticles are of spherical-like structure with diameter of about 40 nm (Figure 3A). HC was chosen for construction of FRET nanoprobe with ARS-FPBA because the absorption peak of ARS-FPBA is at 455 nm, perfectly overlapping with the emission spectra of HC (450 nm) (Figure 3B). In order to prove the occurrence of FRET, we used DSPE-PEG with DSPE-PEG-FPBA, DSPE-PEG-HC, or both DSPE-PEG-HC and DSPE-PEG-FPBA to construct three kinds of polymeric nanoprobes. As shown in Figure 3C, the fluorescence intensity of the ratiometric nanoprobe at 450 nm attributed to HC decreases, while the fluorescence intensity at 600 nm ascribed to ARS-FPBA increases. We obtained a series of FPBA/HC nanoparticles with different ratios of FPBA and HC by changing the amounts of DSPE-PEG-FPBA and DSPE-PEG-HC. Along with increase of the ratio of FPBA to HC, the fluorescence intensity of ARS would increase while that of HC would decrease (Figure S4, Supporting Information). In the presence of H_2O_2, the fluorescence intensity of HC was expected to increase while that of ARS would decrease. In order to magnify the ratiometric change of these two peaks, we chose 200:1 as the optimum concentration ratio and the dual-emission fluorescence intensity ratio (F_{450}/F_{600}) equal to 1.5 approximately. Besides, in order to optimize the concentration of ARS, we measured the fluorescence emission spectra of the polymeric nanoprobe in the presence of ARS by varying ARS concentrations (Figure S5, Supporting Information). There was continuous decrease in fluorescence intensity assigned to HC, meanwhile, the fluorescence intensity of ARS-FPBA increased gradually and tended to be constant with the increase of ARS concentration, indicating that ARS was excessive relative to the polymeric nanoprobe. All the results suggested that FRET-based nanoprobe was successfully prepared. The photostability of the polymeric nanoprobe was tested and the results are shown in Figure 3D. When excited at 405 nm, the emission intensity stays almost unchanged over time, suggesting the good photostability of the polymeric nanoprobe.

The decay profiles of the polymeric nanoprobe before and after conjugation to ARS are shown in Supporting Information Figure S6. The average lifetimes of the polymeric nanoprobe before and after conjugation to ARS are 4.75 and 3.99 ns, respectively. According to eq 3,[42] where τ_{da} and τ_d are the fluorescence lifetimes of a donor in the presence and absence of an acceptor, respectively, the FRET efficiency was estimated to be 0.16 for the polymeric nanoprobe

$$E = 1 - \frac{\tau_{da}}{\tau_d} \quad (3)$$

Good stability is crucial for the application of the polymeric nanoprobe. We thus evaluated the stability of the polymeric nanoprobe in both HEPES buffer solution and serum-containing HEPES. The polymeric nanoprobe shows good dispersity in either serum-free or serum-containing HEPES for 24 h, implying good dispersion stability of the polymeric nanoprobe as confirmed by dynamic light scattering measurement (Figure 4). Using fluorescein as a standard, the fluorescence quantum yield (QY) of the polymeric nanoprobe was calculated to be around 2.4%.

DOI: 10.1021/acs.langmuir.7b00189
Langmuir XXXX, XXX, XXX−XXX

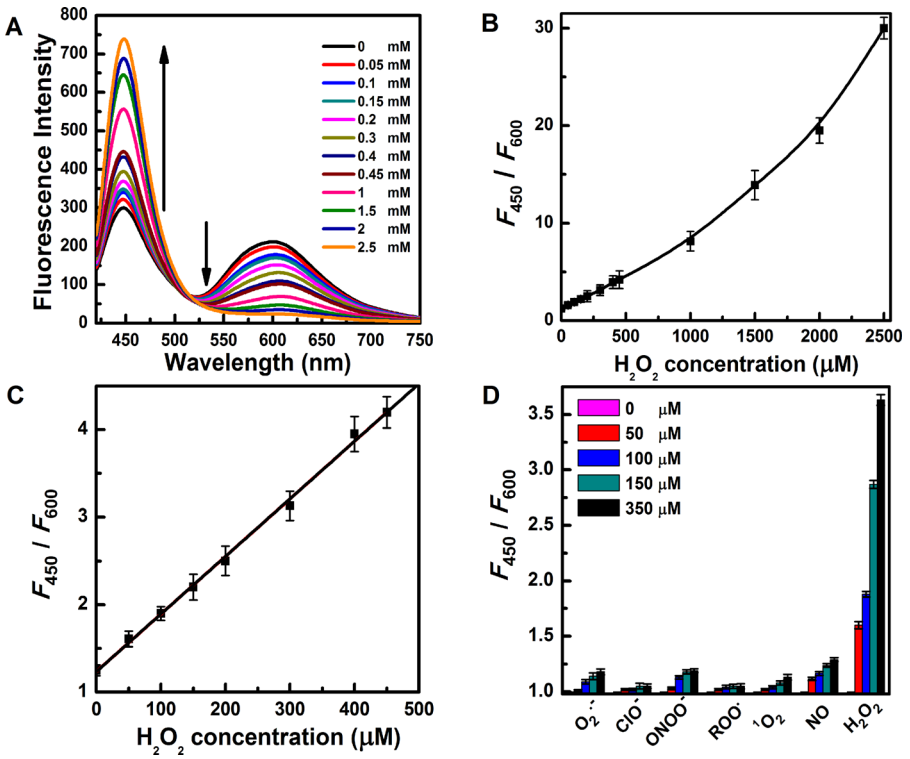

Figure 5. (A) Ratiometric fluorescence response of the polymeric nanoprobe in the presence of different concentrations of H_2O_2. (B) The plot of F_{450}/F_{600} as a function of H_2O_2 concentration. (C) Linear plots of F_{450}/F_{600} at low concentrations of H_2O_2. (D) Selectivity investigation of the polymeric nanoprobe in the presence of different ROS and RNS.

The fluorescence characteristics of the prepared polymeric nanoprobe were then investigated. As expected, the polymeric nanoprobe shows two well-separated fluorescence peaks at 450 and 600 nm upon excitation at 405 nm, which provides the basis for ratiometric fluorescence detection of H_2O_2. Increasing the nanoprobe concentration, the fluorescence intensity ratio (F_{450}/F_{600}) decreased and tended to approach constant at higher concentrations (Figure S7, Supporting Information). Upon the addition of H_2O_2, the fluorescence intensity of peak at 450 nm was attributed to HC increases, while the fluorescence peak at 600 nm ascribed to ARS-FPBA continuously decreases, resulting in the ratiometric response to H_2O_2 (Figure 5A). Figure 5B shows the plot of the fluorescence intensity ratio (F_{450}/F_{600}) as a function of H_2O_2 concentration. The ratio of F_{450}/F_{600} gradually increases along with the increased H_2O_2 concentration. The dual-emission fluorescence intensity ratio increases linearly with the concentration of H_2O_2 between 0 and 500 μM (Figure 5C). The correlation coefficient is 0.9973 with a detection limit of ~0.76 μM (based on a signal-to-noise ratio of 3). We examined the response of the polymeric nanoprobe to other reactive oxygen species (ROS) and reactive nitrogen species (RNS) that have interferences. As shown in Figure 5D, only the addition of H_2O_2 can obviously alter the fluorescence of the polymeric nanoprobe; other ROS and RNS, including superoxide ($O_2^{\bullet-}$), hypochlorite (ClO^-), peroxynitrite ($ONOO^-$), peroxyl radicals ($ROO^{\bullet}$), singlet oxygen ($^1O_2$), and nitric oxide (NO) display small fluorescence response, suggesting high selectivity of the polymeric nanoprobe for H_2O_2 detection. In addition, we investigated the response of the probe to H_2O_2 under different pH (Supporting Information Figure S8), and the result indicated that the probe showed an increased response to H_2O_2 along with increasing solution pH.

We compared our probe with the reported boronate probes in recent years (Table 2). Our probe provides a wide detection range and a comparable detection limit. Meanwhile, the developed probe shows the advantages of facile preparation, high selectivity, and good fluorescence properties.

Table 2. Boronate Probes for the Detection of H_2O_2

probe	detection range (μM)	product λ_{em} (nm)	LOD (μM)	ref
dLys-AgNCs	0.8−200	450/640	0.20	5
T-CuNPs	0.55−110	615	0.55	8
NAC-AuNCs	0.04−6.66	650	0.027	10
probe 1	0−180	410/542	2.0	19
TPE-BO	10−200	500	0.52	40
our work	0−500	450/600	0.76	

Oxidase-triggered oxidation of substrates could produce H_2O_2 as a byproduct. By taking advantage of H_2O_2 as intermediate, the polymeric nanoprobe was configured into biosensor for glucose. The fluorescence spectra of the polymeric nanoprobe with various concentration of glucose in the presence of GOx are depicted in Figure 6A. With increasing amount of glucose, the emission of the polymeric nanoprobe at 600 nm is quenched gradually while that at 450 nm increases dramatically. There is continual increase of F_{450}/F_{600} with the rising of glucose concentration, which indicates that the signal change is related to the glucose concentration (Figure 6B). As shown in Figure 6C, the relationship between F_{450}/F_{600} and glucose concentration presents a good linear response (R^2 = 0.9863) in the range of 0.3−1 mM, with the detection limit of 10 μM (based on a signal-to-noise ratio of 3). Simultaneously, the selectivity of the polymeric nanoprobe toward glucose was

DOI: 10.1021/acs.langmuir.7b00189
Langmuir XXXX, XXX, XXX−XXX

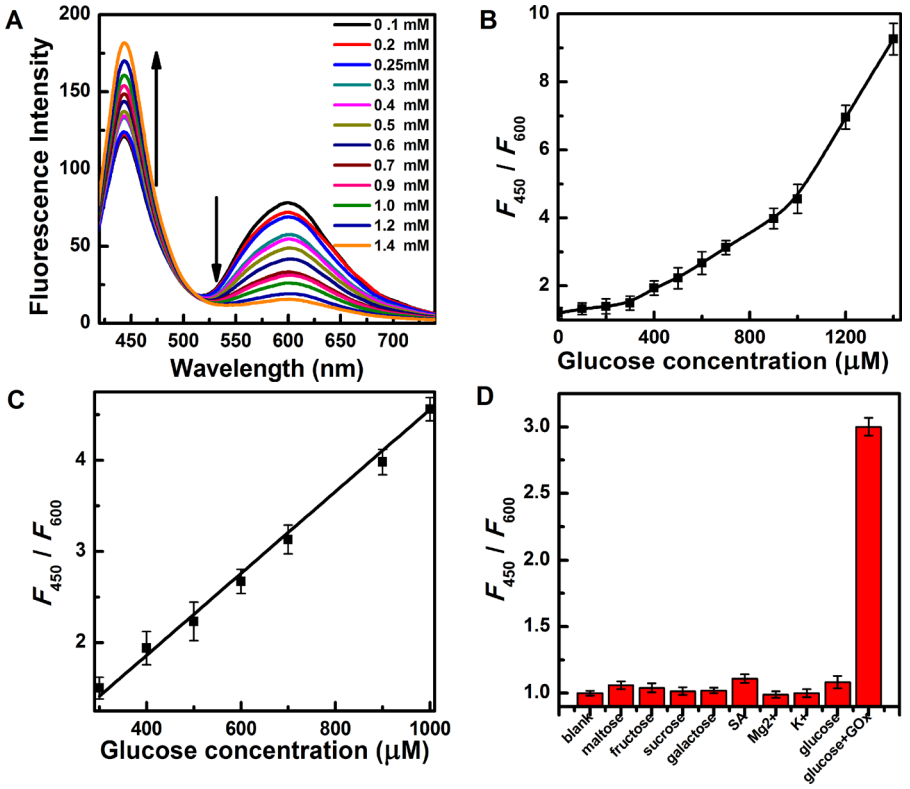

Figure 6. (A) Ratiometric fluorescence response of the polymeric nanoprobe in the presence of different concentrations of glucose in the presence of GOx. (B) The plot of F_{450}/F_{600} as a function of glucose concentration. (C) Linear plots of F_{450}/F_{600} at low concentrations of glucose. (D) Selectivity investigation of the polymeric nanoprobe for the detection of glucose. The concentration of glucose is 1 mM, while those of other interferents are 0.5 mM.

investigated by detecting different carbohydrates and other control substances (Figure 6D). No obvious responses are observed for other related interferents including the high concentration of glucose, which suggests the nanoprobe has superior selectivity for glucose only in the presence of GOx.

The practical applicability of our study was tested by detecting glucose in fetal bovine serum samples. The results are shown in Table 3. It is observed that the recoveries range from

Table 3. Determination of Glucose in FBS Samples

sample	added (mM)	detected (mM)	recovery (%)	RSD (%)
1	0.35	0.37	106	1.0
2	0.60	0.58	97	0.6
3	1.0	0.99	99	1.4

97% to 106%, and the relative standards deviations are from 0.6% to 1.4%. These results indicate that this assay can be further applied to the detection of glucose in real biological samples.

CONCLUSIONS

In summary, we developed a fluorescent nanoprobe by modifying two fluorescent molecules of HC and ARS-FPBA on lipopolymer and preparing nanoprobe by a simple self-assembly method. The nanoprobe displayed selective and ratiometric fluorescence response to H_2O_2. In combination with glucose oxidase, the nanoprobe was further applied to the detection of glucose. The polymeric nanoprobe exhibited remarkable features including facile preparation, long-term stability, highly selective and ratiometric response. Therefore, we believe that this proposed strategy may pave a new way for the construction of a multifunctional polymeric fluorescent nanoprobe and the nanoprobe holds great potential for biochemical study.

ASSOCIATED CONTENT

Supporting Information

The Supporting Information is available free of charge on the ACS Publications website at DOI: 10.1021/acs.langmuir.7b00189.

Additional schemes, figures, and tables (PDF)

AUTHOR INFORMATION

ORCID

Zhiai Xu: 0000-0002-4391-2507

Notes

The authors declare no competing financial interest.

ACKNOWLEDGMENTS

Financial supports by the National Natural Science Foundation of China (No. 21675055, 31622025, 21375040, 21635003) are greatly appreciated.

REFERENCES

(1) Abo, M.; Urano, Y.; Hanaoka, K.; Terai, T.; Komatsu, T.; Nagano, T. Development of a highly sensitive fluorescence probe for hydrogen peroxide. *J. Am. Chem. Soc.* **2011**, *133*, 10629−10637.

(2) Rhee, S. G. Cell signaling. H_2O_2, a necessary evil for cell signaling. *Science* **2006**, *312*, 1882−1883.

DOI: 10.1021/acs.langmuir.7b00189
Langmuir XXXX, XXX, XXX−XXX

(3) Finkel, T. Signal transduction by reactive oxygen species. *J. Cell Biol.* **2011**, *194*, 7−15.
(4) Song, Z.; Kwok, R. T. K.; Ding, D.; Nie, H.; Lam, J. W. Y.; Liu, B.; Tang, B. An AIE-active fluorescence turn-on bioprobe mediated by hydrogen-bonding interaction for highly sensitive detection of hydrogen peroxide and glucose. *Chem. Commun.* **2016**, *52*, 10076−10079.
(5) Liu, F.; Bing, T.; Shangguan, D.; Zhao, M.; Shao, N. Ratiometric fluorescent biosensing of hydrogen peroxide and hydroxyl radical in living cells with lysozyme−silver nanoclusters: lysozyme as stabilizing ligand and fluorescence signal unit. *Anal. Chem.* **2016**, *88*, 10631−10638.
(6) Alfadda, A. A.; Sallam, R. M. Reactive oxygen species in health and disease. *J. Biomed. Biotechnol.* **2012**, *2012*, 1−14.
(7) Kamat, P. J.; Devasagayam, T. P. A. Oxidative damage to mitochondria in normal and cancer tissues, and its modulation. *Toxicology* **2000**, *155*, 73−82.
(8) Mao, Z.; Qing, Z.; Qing, T.; Xu, F.; Wen, L.; He, X.; He, D.; Shi, H.; Wang, K. Poly(thymine)-templated copper nanoparticles as a fluorescent indicator for hydrogen peroxide and oxidase-based biosensing. *Anal. Chem.* **2015**, *87*, 7454−7460.
(9) Zeng, H.; Qiu, W.; Zhang, L.; Liang, R.; Qiu, J. Lanthanide coordination polymer nanoparticles as an excellent artificial peroxidase for hydrogen peroxide detection. *Anal. Chem.* **2016**, *88*, 6342−6348.
(10) Deng, H.; Wu, G.; He, D.; Peng, H.; Liu, A.; Xi, X.; Chen, W. Fenton reaction-mediated fluorescence quenching of N-acetyl-L-cysteine-protected gold nanoclusters: analytical applications of hydrogen peroxide, glucose, and catalase detection. *Analyst* **2015**, *140*, 7650.
(11) Fu, Y.; Yao, J.; Xu, W.; Fan, T.; Jiao, Z.; He, Q.; Zhu, D.; Cao, H.; Cheng, J. Schiff base substituent-triggered efficient deboration reaction and its application in highly sensitive hydrogen peroxide vapor detection. *Anal. Chem.* **2016**, *88*, 5507−5512.
(12) Yang, Y.; Zhao, Q.; Feng, W.; Li, F. Luminescent chemodosimeters for bioimaging. *Chem. Rev.* **2013**, *113*, 192−270.
(13) Kim, J. S.; Quang, D. T. Calixarene-derived fluorescent probes. *Chem. Rev.* **2007**, *107*, 3780−3799.
(14) Chinen, A.; Guan, C.; Ferrer, J.; Barnaby, S.; Merkel, T.; Mirkin, C. Nanoparticle probes for the detection of cancer biomarkers, cells, and tissues by fluorescence. *Chem. Rev.* **2015**, *115*, 10530−10574.
(15) Kim, H. N.; Ren, W. X.; Kim, J. S.; Yoon, J. Fluorescent and colorimetric sensors for detection of lead, cadmium, and mercury ions. *Chem. Soc. Rev.* **2012**, *41*, 3210−3244.
(16) Chen, X.; Pradhan, T.; Wang, F.; Kim, J. S.; Yoon, J. Fluorescent chemosensors based on spiroring-opening of xanthenes and related derivatives. *Chem. Rev.* **2012**, *112*, 1910−1956.
(17) Liu, C.; Shao, C.; Wu, H.; Guo, B.; Zhu, B.; Zhang, X. A fast-response, highly sensitive and selective fluorescent probe for the ratiometric imaging of hydrogen peroxide with a 100 nm red-shifted emission. *RSC Adv.* **2014**, *4*, 16055−16061.
(18) Albers, A. E.; Okreglak, V. S.; Chang, C. J. A FRET-based approach to ratiometric fluorescence detection of hydrogen peroxide. *J. Am. Chem. Soc.* **2006**, *128*, 9640−9641.
(19) Zhu, B.; Jiang, H.; Guo, B.; Shao, C.; Wu, H.; Du, B.; Wei, Q. A highly selective ratiometric fluorescent probe for hydrogen peroxide displaying a large emission shift. *Sens. Actuators, B* **2013**, *186*, 681−686.
(20) Vikesland, P. J.; Wigginton, K. R. Nanomaterial enabled biosensors for pathogen monitoring - a review. *Environ. Sci. Technol.* **2010**, *44*, 3656−3669.
(21) Alivisatos, P. The use of nanocrystals in biological detection. *Nat. Biotechnol.* **2004**, *22*, 47−52.
(22) Lim, E. K.; Kim, T.; Paik, S.; Haam, S.; Huh, Y. M.; Lee, K. Nanomaterials for theranostics: recent advances and future challenges. *Chem. Rev.* **2015**, *115*, 327−394.
(23) Kataoka, K.; Harada, A.; Nagasaki, Y. Block copolymer micelles for drug delivery: design, characterization and biological significance. *Adv. Drug Delivery Rev.* **2001**, *47*, 113−131.
(24) Talelli, M.; Rijcken, C. J. F.; van Nostrum, C. F.; Storm, G.; Hennink, W. E. Micelles based on HPMA copolymers. *Adv. Drug Delivery Rev.* **2010**, *62*, 231−239.
(25) Duncan, R. The dawning era of polymer therapeutics. *Nat. Rev. Drug Discovery* **2003**, *2*, 347−360.
(26) Nishiyama, N.; Kataoka, K. Current state, achievements, and future prospects of polymeric micelles as nanocarriers for drug and gene delivery. *Pharmacol. Ther.* **2006**, *112*, 630−648.
(27) Shi, Y.; van Nostrum, C. F.; Hennink, W. E. Interfacially hydrazone cross-linked thermosensitive polymeric micelles for acid-triggered release of paclitaxel. *ACS Biomater. Sci. Eng.* **2015**, *1*, 393−404.
(28) Kataoka, K.; Harada, A.; Nagasaki, Y. Block copolymer micelles for drug delivery: design, characterization and biological significance. *Adv. Drug Delivery Rev.* **2001**, *47*, 113−131.
(29) Yang, R.; Meng, F.; Ma, S.; Huang, F.; Liu, H.; Zhong, Z. Galactose-decorated cross-linked biodegradable poly(ethylene glycol)-b-poly(ε-caprolactone) block copolymer micelles for enhanced hepatoma-targeting delivery of paclitaxel. *Biomacromolecules* **2011**, *12*, 3047−3055.
(30) Torchilin, V. P. Micellar nanocarriers: pharmaceutical perspectives. *Pharm. Res.* **2007**, *24*, 1−16.
(31) Springsteen, G.; Wang, B. Alizarin Red S. as a general optical reporter for studying the binding of boronic acids with carbohydrates. *Chem. Commun.* **2001**, 1608−1609.
(32) Springsteen, G.; Wang, B. A detailed examination of boronic acid−diol complexation. *Tetrahedron* **2002**, *58*, 5291−5300.
(33) Sun, X.; Lacina, K.; Ramsamy, E. C.; Flower, S. E.; Fossey, J. S.; Qian, X.; Anslyn, E. V.; Bull, S. D.; James, T. D. Reaction-based indicator displacement assay (RIA) for the selective colorimetric and fluorometric detection of peroxynitrite. *Chem. Sci.* **2015**, *6*, 2963−2967.
(34) Wang, L.; Qiao, J.; Li, H.; Hao, J.; Qi, L.; Zhou, X.; Li, D.; Ni, Z.; Mao, L. Ratiometric fluorescent probe based on gold nanoclusters and alizarin red-boronic acid for monitoring glucose in brain microdialysate. *Anal. Chem.* **2014**, *86*, 9758−9764.
(35) Billingsley, K. L.; Balaconis, M. K.; Dubach, J. M.; Zhang, N.; Lim, E.; Francis, K. P.; Clark, H. A. Fluorescent nano-optodes for glucose detection. *Anal. Chem.* **2010**, *82*, 3707−3713.
(36) Chen, P.; Wan, L.; Ke, B.; Xu, Z. Honeycomb-patterned film segregated with phenylboronic Acid for glucose sensing. *Langmuir* **2011**, *27*, 12597−12605.
(37) Tomsho, J. W.; Benkovic, S. J. Elucidation of the mechanism of the reaction between phenylboronic acid and a model diol, Alizarin Red S. *J. Org. Chem.* **2012**, *77*, 2098−2106.
(38) Xu, Z.; Morita, K.; Sato, Y.; Dai, Q.; Nishizawa, S.; Teramae, N. Label-free aptasensor for adenosine using abasic site-containing DNA and a nucleobase-specific fluorescent ligand. *Chem. Commun.* **2009**, *42*, 6445−6447.
(39) Xu, Z.; Yusuke, S.; Seiichi, N.; Norio, T. Signal-off and signal-on design for label-free aptasensor based on target-induced self-assembly and abasic site-binding ligands. *Chem. - Eur. J.* **2009**, *15*, 10375−10378.
(40) Zhang, W.; Liu, W.; Li, P.; Huang, F.; Wang, H.; Tang, B. Rapid-response fluorescent probe for hydrogen peroxide in living cells based on increased polarity of C-B bonds. *Anal. Chem.* **2015**, *87*, 9825−9828.
(41) Lippert, A. R.; Van De Bittner, G. C.; Chang, C. J. Boronate oxidation as a bioorthogonal reaction approach for studying the chemistry of hydrogen peroxide in living systems. *Acc. Chem. Res.* **2011**, *44*, 793−804.
(42) Biju, V.; Itoh, T.; Baba, Y.; Ishikawa, M. Quenching of photoluminescence in conjugates of quantum dots and single-walled carbon nanotube. *J. Phys. Chem. B* **2006**, *110*, 26068−26074.

DOI: 10.1021/acs.langmuir.7b00189
Langmuir XXXX, XXX, XXX−XXX